

Characterization of Magnetic Communication Through Human Body

Rajpreet K Gulati*, Sayemul Islam†, Amitangshu Pal‡, Krishna Kant*, Albert Kim†

*Computer and Information Sciences, Temple University, Philadelphia, PA 19122, USA

†Electrical and Computer Engineering, Temple University, Philadelphia, PA 19122, USA

‡Computer Science and Engineering, Indian Institute of Technology Kanpur, Kanpur, India

Abstract—Biomedical systems of implanted miniaturized sensors and actuators interconnected into an intra-body area network could revolutionize treatment options for chronic diseases afflicting internal organs. Considering the well-understood limitations of radio frequency (RF) propagation in the human body, we have explored magnetic resonance (MR) coupling for both communications and energy transfer through the body. In this paper, we have discussed the design and implementation of a software-defined prototype using Universal Software Radio Peripheral (USRP) boards. We have reported experimental results on the achieved packet error rates at different positions through-the-body distances and packet sizes. We have observed experimentally that the MR signal propagates through the body substantially better than in the air, and can provide a practical means for energy transfer and communications in intra-body networks. It also works better than the better understood galvanic coupling.

Index Terms—Magnetic resonance coupling; magnetic communication; intra-body sensor network; wireless power transfer;

I. INTRODUCTION

With an aging population and increasing pollution in most of the countries, chronic diseases are becoming quite common. For example, in the US, approximately 45%, or 133 million people suffer from at least one chronic disease [1] and more than 50% of older adults suffer from ≥ 3 chronic conditions [2]. Many of these can be actively managed using implantable medical devices (IMDs) [3]. IMDs have made significant improvements in recent years, with advancements in integrated circuits, MEMS, wireless systems, and battery technologies. IMDs have two related functions: (a) to measure disease-related parameters and control the delivery of drugs or physiological stimuli (e.g., electric shock), and (b) to perform physiological health monitoring such as implanted cardio-defibrillators, implantable neuro-stimulators, etc. to assist physicians in providing advice to the patient regarding a change in type or quantity of medications, to avoid certain foods and a certain type of movements, etc.

In some chronic diseases or natural function defects of organs, the formation of a therapeutic network of multiple sensors and actuators in the body can achieve unprecedented management, such as a spinal neuro-modulator based on bladder pressure monitoring to control overactive bladder through implanted pressure sensor and micro-electrode mediated nerve recording to monitor urine output [4]; effectively control the pacemaker through monitoring of pH, oxygen, respiration, activity, and drug infusion [5]; or through a brain-computer

interface via implantable microelectrode arrays (where the number of channels can exceed 100) [6].

All these applications require robust and highly energy-efficient means of *Human Body Communication* (HBC), i.e., communication between intra-body nodes (or on body nodes entirely through the body media). The limitations of radio frequency (RF) communications for HBC are well known [7], [8], and several alternative technologies have been proposed, but their relative merits in terms of data transfer are not very clear. Exploring this aspect experimentally forms the key contribution of this paper. The HBC signal propagation methods can be classified as galvanic coupling (GC) [9], [10], capacitive coupling (CC) [11], [12], and magnetic resonance coupling (MR) [13], [14].

Galvanic HBC couples the signal to the human body through a pair of electrodes in contact with the skin that serves as a transmitter (T_x) and receiver (R_x) respectively. The human body has a relatively low conductivity, so the signal flowing between the transmit and receive electrodes is rather small [9], [10]. Instead, due to very short spacing between the positive and negative terminals on each end, much of the current flows locally. Thus GC coupling does not provide a very efficient way of energy transfer or communication across the body.

The capacitive coupling (also known as electrostatic coupling) uses T_x and R_x electrodes. The signal electrodes are capacitively attached to the body while the ground electrodes are left floating, creating a capacitance with the environment (earth, air, or other objects in the surrounding). Capacitive coupling is heavily affected by the local electrical environment [12], [15], making it inefficient for wearable and implantable applications. Therefore, we will not consider it further in this paper.

The magnetic resonance coupling refers to the signal coupling between the T_x and R_x coils via magnetic flux. Both transmitter and receiver consist of an identical inductive coil in parallel with an identical capacitor to form a resonant LC circuit (an electric circuit consists of an inductor, represented by the letter L, and a capacitor, represented by the letter C, connected) that can transfer energy quite efficiently at the resonance frequency. The spectral range most frequently utilized in MR coupling spans from about 100KHz to 50 MHz [16]. Although MR coupling has been studied in the past, there are no comprehensive results for packet loss rate

as a function of packet size and in-body distance. In this paper, we explore these different technologies experimentally.

The key contribution of the paper is to experimentally study the performance of packet transmission through the body via magnetic resonance (MR) coupling. We show that the MR coupling works much better through the body than in the air and has superior performance as compared to galvanic coupling. Also, at large enough distances where some packets are lost, the packet error rate is rather insensitive to the packet size, thereby indicating that the much of the error is incurred in framing rather than the rest of the packet.

The rest of the paper is organized as follows. Section II discusses the related work. Section III discusses the experimental setup. Section IV discusses the results and section V then concludes the discussion.

II. RELATED WORK

In HBC, an electromagnetic signal is coupled into the body through electrodes and is tapped from another part of the body using similar electrodes. Several coupling methods have been discussed in the literature. In the following we discuss some related literature on galvanic and MR coupling methods, which are our primary focus in this paper.

A. Galvanic coupling

Developing communication mechanism through human body is well researched. Handa et al. reported a low-power HBC system in as early as 1997 [17]. An ECG signal from the chest was transformed into a micro-Ampere electric current and sensed by electrodes on the wrist. The electrodes were in direct contact with the body, causing galvanic coupling. This system utilized only $8\mu\text{W}$. The results show that galvanic coupling HBC can transmit data with low transmission power. In 1998, Lindsey et al. [18] examined HBC between an implanted device and an external data collection system. The approach used two 0.38 mm platinum electrodes spaced by 2.5 mm to inject sinusoidal currents of 2–160 kHz and 1–3 mA into a cadaver limb. The voltage variations were measured using EMG electrodes on the leg. The signal attenuation was 37–47 dB. This prototype uses galvanic coupling HBC to transport data between implanted devices and body surface sensors. The tissue surrounding the transmitter generates a high ionic current. The current diminishes with distance from the transmitter due to tissue resistance [19]. At the receiver, a high-gain differential amplifier detects the current's electric potential. Most existing studies and prototypes involve human limbs. Based on ionic current propagation, the operating frequency should be low (1 MHz [20]), which has the added advantage of very low signal leakage through the air [21].

B. Magnetic resonance coupling

Magnetic resonance coupling (MRC) is used largely for wireless energy transfer. Reference [16] proposes near-field wireless electrical energy transmission between two coils wrapped around the body to drive the field propagation. The magnetic field mentioned in [16] has a wavelength of 2.3m,

which may interfere with other nearby devices' magnetic fields. Simulation based analysis for MR coupling is performed in [22], with encouraging results for transmission properties. The distribution of magnetic fields is modeled around the arm, to study and predict the arm movement's effect on the communication. Attenuation is noticed when torso comes in between transmitter and receiver. Theory and challenges for traditional near-field resonant inductive coupling for implantable applications have been discussed in [23]. In [24] MR coupling system using resonators with grounded loops is discussed. Grounded loop reduces the leakage of the electric field, resulting in less interaction with the human body.

Although the basic MR coupling method has been studied extensively in the literature, we still need to understand it in the context of the HBC environment. In particular, we need to obtain packet delivery performance with respect to the transceiver distance, and passage through different parts of the body. We also compare these two coupling methods through extensive on body experiments.

III. EXPERIMENT SETUP

Studying packet delivery/corruption characteristics requires building transceiver boards; in the following we describe our basic transceiver design using a software defined radio platform along with other necessary components, e.g., D/A, A/D converters, amplifier, antennas etc.

A. Instruments

There are many SDR (software-defined radio) development platforms [25] [26] that utilize FPGAs or specialized CPUs for high-sample-rate digital signal processing. We chose USRP [25] because of its cheap cost and widespread use in academics and industries. A motherboard and two daughterboards comprise the USRP N210. The primary processing unit is the motherboard, which includes AD/DA converters (a dual 100 MSPS 14-bit ADC and a dual 400 MSPS 16-bit DAC) and an FPGA unit (Spartan 3A-DSP 3400). The daughterboards are radio frequency (RF) front ends that connect the device to a transmitter or receiving antennas. We utilize LFTX and LFRX daughterboards that run from DC to 30 MHz, which covers frequency ranges that we are interested in.

We used USRP N210, LFTX and LFRX daughterboards to measure the data rate of the packet received between transmitter and receiver. Electrodes (for galvanic) and coils (for MR) were connected to the USRP N210 respectively for each experiment. We used the transmission frequency of 13.56 MHz for both the coupling methods, which is most frequently used for MR coupling and corresponds to RFID frequency [27]. The transmission power is maintained at 0 dBm (1 mW) throughout the study. Power received was measured to determine the signal attenuation for both the galvanic and magnetic resonance coupling methods. The measurement devices were carefully calibrated before each experiment to ensure accurate measurements. Fig. 1 shows the transmit/receive antennas for the coupling methods.

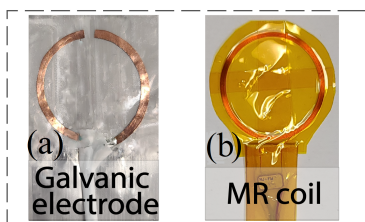


Fig. 1. Transmit (and receive) antennas for (a) galvanic and (b) MR coupling methods.

For galvanic coupling, an electrical insulator is inserted in the middle of two half-circular conductive copper sheets (width = 1.6 mm, dia = 33.2 mm, thickness = 0.1 mm) as shown in Fig. 1(a), which serve as our electrodes (T_x and R_x). Bio-compatible polypropylene film-based pressure-sensitive adhesive (PSA) tape (ARseal 90880, Adhesives Research) is used to attach galvanic electrodes directly to the skin. This increases the conductivity and eliminates air gaps.

For the MR coupling experiments, commercially available RFID coils (Zycoil Electronic Co.) as shown in Fig.1(b) coupled with a capacitor as T_x and R_x were used. The inductance (made out of 10 turns of 34 AWG, polyimide insulated copper wire, dia = 33.2 mm) of $9.27 \mu\text{H}$ is used with the planar coil. It is connected in parallel with a 14.86 pF capacitor, forming an LC circuit with a resonance frequency of 13.56 MHz. Two other MR coils were also used for comparison purposes as listed in Table II. The transmitter and receiver coil were covered by a specialized magnetic shielding film (WMF200, Woremor) to minimize magnetic interference from nearby electronic equipment and over-the-air transmission [28].

B. Packet Transmission Technique

For narrow-band transmission, the 13.56 MHz carrier can be digitally modulated by switching signal (on-off keying; OOK), frequency (frequency shift keying; FSK), or carrier phase (phase shift keying; PSK). The bandwidth of all three technologies is approximately equal to the signaling rate. Phase shift keying is a modulation format widely used in low-bit-rate applications with moderate error performance. Due to its simplicity and low hardware cost, Binary Phase shift keying (BPSK) seems ideal. PSK detection typically uses two matched band-pass filters tuned to the carrier frequency and phase shift, as well as a symbol detector and decision circuit. Coherent PSK detection is better when using synchronous detection noise suppression, but must be synchronized with the transmitter's frequency. The best solution focuses on high receiver sensitivity and simplicity at a reasonable data rate.

C. Wireless transmission using USRP and GNU radio

A series of signal processing blocks can be combined to create flow graphs in the GNU Radio project. These blocks are built using the C++ or Python programming language, which has several benefits, such as simple installation, connectivity, and the easy generation of GUIs. Existing GNU Radio blocks span different applications from basic math to sophisticated

digital filters, modulators/demodulators, channel codecs, voice codecs, etc. Input/output blocks are a subclass of blocks. They provide a connection to the actual world; the most well-known of them is the UHD (USRP hardware driver). The UHD blocks are designed to make use of the USRP and transmit/receive signals via a wireless channel. The detailed block diagram

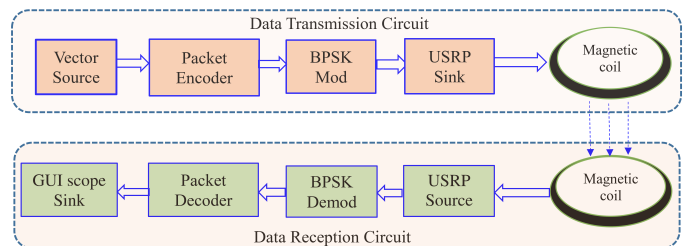


Fig. 2. Block diagram of wireless transmission with USRP board and GNU radio.

of GNU radio is shown in Fig. 2. Vector source generates a string of bits; the output of the vector source is connected to the packet encoder. After the encoder, the encoded data is sent to the PSK modulator. The PSK modulator was configured as a BPSK modulator. The signal from the BPSK modulator is sent to the USRP Sink block which is responsible for interacting with the USRP. This block has several parameters that are used by the hardware, such as, center frequency and the antenna type used on the daughter-board. We used SMA cables to connect the USRP board with transceivers.

At the receiver end the USRP source output is connected to the PSK Demodulator block that demodulates the PSK signal (BPSK in this example) and recovers the encoding data. After the demodulation, the encoded data is sent to the packet decoder block, which decodes the data and outputs the bits.

D. Experimental protocol with human subjects

Except for some air experiments, all experiments in this study were conducted on the human body. The experimental methods were approved by the department IRB (Institutional Review Board) and regulatory affairs. We conducted RSSI experiments with several volunteers of different ages, the body builds, and gender. These results may be found in [29] and are not included here, since our focus in this paper is on packet delivery issues and power received using USRP boards. Packet delivery and power received have not been studied in [29]. We found that person-to-person variations are quite small in all cases; therefore, all packet transmission experiments conducted for this paper are for a single volunteer. We also found that the body movement or different poses do not have much impact on the signal strength, and are thus not expected to affect packet delivery. Therefore, the results reported here are for a volunteer in a standing position as discussed earlier.

Two configurations were used to conduct experiments. In the first configuration, the position used was with the arms extended to the sides of the body horizontally. The arms were straight. The transmitter was placed on the left hand.

TABLE I

COMPARISON OF PACKET RECEIVED IN TWO CONFIGURATIONS. (NUMBER OF TRANSMITTED PACKETS $T = 1000$)

Distance	Left hand to right hand (L)	Shoulder to feet (R)	% difference, $D= L-R \times 100 / T$
30 cm	1000	1000	0
60 cm	1000	1000	0
90 cm	750	752	0.2
120 cm	20	19	0.1

In successive experiments, the receiver was moved towards the right arm in steps of 5 cms. In the second configuration, the transmitter was placed on the shoulder, and the receiver was moved in steps of 5 cm down towards the feet on the body. In both these configurations, the human subject was in standing pose on a vinyl floor.

We first tried to compare the packet delivery of MR coupling using these two configurations. In a single run, 1000 packets with 56 Bytes were sent from the transmitter to the receiver. The results from this experiments are listed in Table I. From this table we can observe that the results from both of these configurations are almost similar (within $\sim 2\%$ difference in packet delivery) w.r.t the transceiver distance.

E. Frame Structure

We used the packet frame structure shown in Fig. 3 to send the data packets between the transmitter and receiver. The minimum packet size used was 56B.

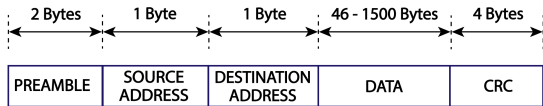


Fig. 3. Illustration of the used frame structure with different fields.

The preamble is a 2-Byte field and should be adequate for framing. For intrabody networks, 256 nodes should be adequate; therefore, we use only 1-byte each for source and destination addresses. The data payload size varies between 46 and 1500 bytes. The cyclic redundancy check (CRC) is a standard 32-bit CRC used for integrity checking.

By a careful comparison between sent and received data, we found that in all cases, the CRC was able to detect the error; therefore, all packets received without the CRC error represent packets that do not suffer from any bit flips.

F. Safety considerations

Unregulated, non-static electromagnetic fields may cause adverse health effects on humans [30] especially when under long-term exposure. In this paper, we strictly maintained the transmission power output of the USRP boards at 0 dBm (1 mW). For 13.56 MHz frequency, the magnetic flux density in all our experiments was maintained at less than $1 \mu T$, which is well under the reported safety recommendation by IEEE standard [31].

IV. RESULTS AND DISCUSSION

A. Performance comparison using different MR coils

We first investigated how different MR coil design affects the signal transmission performance. Considering the magnetic flux density, inductance, and mutual coupling factors, we developed three different MR coils; we denote these coils as A, B, C as shown in Fig. 4. For this experiment, we set the resonance frequency for all the coils at 13.56 MHz.

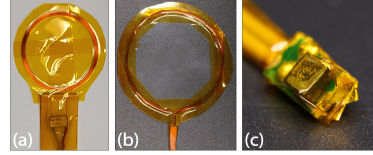


Fig. 4. Illustration of the MR coils A-C.

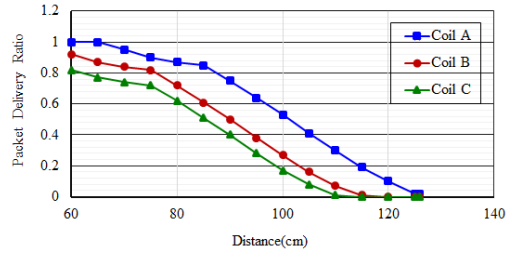


Fig. 5. MR coils A-C and their performances in terms of packet delivery ratio.

Table II shows the design specifications of these coils. As mentioned before, matched T_x and R_x coils were placed in the forearms of a subject and covered by the magnetic shielding films as shown in Fig. 4. We sent a sequence of 1000 packets at a time, each 56B in size. Fig. 5 shows the variation of packet delivery ratio with different transceiver distances. As expected, the MR coil A, which has the biggest overall size (33.2 mm diameter and 10 turns) resulted in the best transmission performance. From Fig. 5, we can observe that coil A delivered 100% packets at 65 cm and 50% at 100 cm. On the other hand, coil B, which has 48 mm diameter but only 2 turns, showed poorer performance, whereas coil C performed the worst (50% packets received at 85 cm).

TABLE II
MR COIL SPECIFICATIONS (RESONANCE FREQUENCY = 13.56 MHz)

Parameter	Coil A	Coil B	Coil C
1. Dimension	Dia = 33.2 mm $N = 10$ turns	Dia = 48 mm $N = 2$ turns	$L = 3.2$ mm $W = 2.0$ mm
2. Inductance	$9.27 \mu H$	$950 nH$	$15 nH$
3. Capacitance	$14.86 pF$	$145 pF$	$9.2 nF$
4. Magnetic flux density	$0.962 \pm 0.01 \mu T$	$0.224 \pm 0.001 \mu T$	$0.074 \pm 0.004 \mu T$

B. MR coupling vs. other coupling methods

We next compared the performance of through the body MR and galvanic coupling methods. Fig. 6 illustrates the variation of packet delivery ratio with different transceiver distances using these two coupling methods. For comparison purpose, the result on MR transmission through the air is also

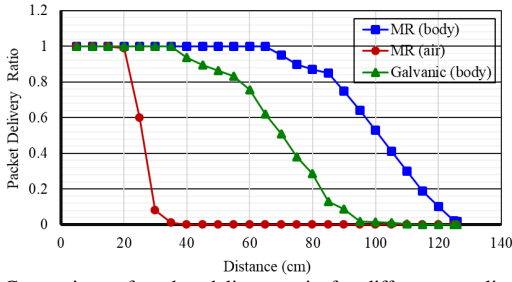


Fig. 6. Comparison of packet delivery ratio for different coupling methods with different transceiver distances.

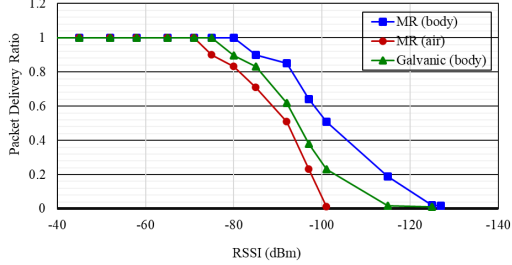


Fig. 7. Comparison of packet delivery ratio for different coupling methods with different RSSI.

shown. From Fig. 6, we can observe that the transmission range using through the body MR communication is much more efficient than that of air media, i.e. human body forms a better transmission media for MR transmission than air. It is also observed that the MR transmission is significantly better than galvanic; this is partly because much of the current flow in the case of galvanic coupling is local due to the way this technology works. It is also worth noticing that with MR, there is almost no packet drop for up to 65 cm distance, which would be plenty for most intra-body network applications. As stated above, these results are for 1 mW of transmitted signal in intra-body applications. It would be desirable to lower the power further to conserve the battery, which would reduce the range accordingly.

Fig. 7 illustrates the variation of the packet delivery ratio and the received signal strength indicator (RSSI) at the receiver. From this figure we can observe that in case of through the body communication, to achieve 100% packet delivery, the RSSI can be down to -80 dBm for MR coupling but only -75 dBm for galvanic coupling. The corresponding number for air is -70 dBm. Typically in a homogeneous medium, the PDR vs. RSSI generally does not depend on the media characteristics; however, from our observations this is not the case for the body since it is a highly non-homogeneous media.

C. Packet Delivery Ratio vs. Packet Size

We next conducted experiments to assess the packet delivery ratio (PDR) vs. the packet size as well, using MR coupling for human body communication. Fig. 8 shows the packet error rate (PER) for air transmission of MR. The experiments used four different packet sizes (56, 100, 200, 300 and 400 Bytes) with varying payload size as depicted in Fig. 3. The received packets were identified as erroneous if they did not pass the 32-bit CRC as mentioned earlier. However, the much more

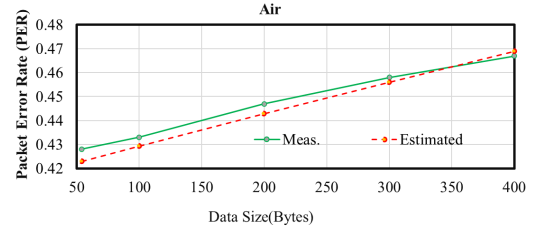


Fig. 8. Measured and Estimated PER vs. packet size in air media.

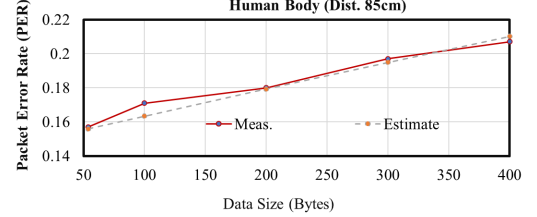


Fig. 9. Measured and estimated PER vs. packet size in body media with transceiver distance of 85 cm.

significant reason for not receiving the packet is the error in the received preamble bits.

Any bit flip or unrecognized symbol in the preamble will miss the entire packet. (We ensured that the data in the packets did not contain the preamble pattern). As expected, the PER increases with the packet size, however, the increase is quite marginal from 56 bytes to 400 bytes. As surmised and extensively verified in [32], the errors in the preamble and data parts should be considered separately and could be quite different, with preamble error dominating the packet loss characteristics. Thus, by assuming that the errors are independent at the bit level, and using two different bit error rates (BERs) for preamble and data (denoted p_p and p_d respectively), we can estimate the PER as a function of packet size. Here we did the opposite, we estimated p_p and p_d to best fit the observed PER, and then estimated PER as follows:

$$\text{PER}_{\text{est}} = 1 - (1 - p_p)^{L_p} (1 - p_d)^{L_d} \quad (1)$$

where L_p and L_d are the lengths (in bits) of the preamble and data. In estimating p_p and p_d we made use of observed packets received with and without CRC errors; with preamble BER p_p considered independent of packet length.

Fig. 8 shows the measured BER (solid line) and estimated PER (dotted line) at 20cm distance. It is seen that the fit is excellent. Figs. 9-11 show a similar estimation procedure for the human body at 3 different distances, namely 85 cm, 100 cm, and 115 cm. These 3 distances were chosen based on Fig. 6 to cover different levels of delivery ratios. For each distance, we estimated the p_p and p_d from the measured (body) data. The calculation shows that the p_d is very small and rather insensitive to the distance, but p_p increases rapidly with the distance. It is again seen that the fit is excellent in all 3 cases.

V. CONCLUSIONS AND FUTURE WORK

In this paper, we performed an experimental study of magnetic resonance coupling-based communication for use by

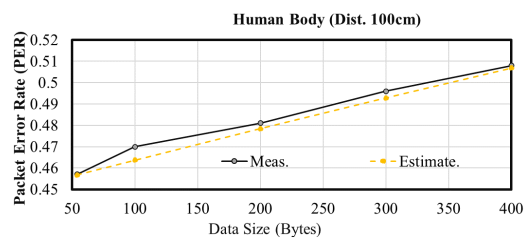


Fig. 10. Measured and estimated PER vs. packet size in body media with transceiver distance of 100 cm.

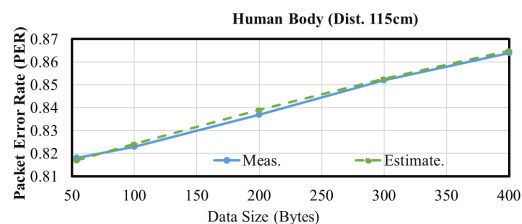


Fig. 11. Measured and estimated PER vs. packet size in body media with transceiver distance of 115 cm.

on-body and intra-body nodes with the signal being communicated through the body. We showed that the mechanism works much better for transmission through the body than through the air. In particular, it is seen that at 1 mW transmitted power, the packets can be received without any error for up to 65 cm distance. We also compared MR transmission against galvanic coupling and showed that MR works significantly better.

We modeled the packet error rate as a function of packet length and found that the error rate increases very slowly with the packet size. A simple error model, where all bits are assumed to be flipped independently, but the preamble BER is much higher than the data BER fits the experimental results extremely well. However, this does not necessarily validate the independence assumption. In the future, we will examine this issue further and accordingly explore how to improve the performance, including forwarding error correction.

ACKNOWLEDGEMENT

The project was supported by the National Science Foundation (NSF) grants ECCS-2029077 (PI A. Kim), and CNS-1844944 (PI K. Kant). The authors would also like to acknowledge Michael Domic from Temple University (Philadelphia, PA, USA) for their help with the experiments.

REFERENCES

- [1] L. P. Fried, "America's health and health care depend on preventing chronic disease," https://www.huffingtonpost.com/entry/americas-health-and-healthcare-depends-on-preventing_us_58c0649de4b070e55af9eade, March 2017.
- [2] A. Tinker, "How to improve patient outcomes for chronic diseases and comorbidities," <http://www.healthcatalyst.com/wp-content/uploads/2014/04/How-to-Improve-Patient-Outcomes.pdf>, 2017.
- [3] H. Tung *et al.*, "A mobility enabled inpatient monitoring system using a zigbee medical sensor network," *Sensors*, vol. 14, pp. 2397–2416, 2014.
- [4] A. Mendez *et al.*, "Estimation of bladder volume from afferent neural activity," *IEEE Transactions on Neural Systems and Rehabilitation Engineering*, vol. 21, pp. 704–715, 2013.
- [5] R. A. Normann *et al.*, "Clinical applications of penetrating neural interfaces and Utah electrode array technologies," *Journal of neural engineering*, vol. 13, p. 061003, 2016.
- [6] R. G. HAUSER, "Techniques for improving cardiac performance with implantable devices," *Pacing and Clinical Electrophysiology*, vol. 7, pp. 1234–1239, 1984.

- [7] D. Werber *et al.*, "Investigation of RF transmission properties of human tissues," *Advances in Radio Science*, vol. 4, pp. 357–360, sep 2006.
- [8] H.-Z. T. Chen *et al.*, "A study of rf power attenuation in bio-tissues," *Journal of Medical and Biological Engineering*, vol. 24, pp. 141–146, 2004.
- [9] X. fang Li *et al.*, "Galvanic coupling type intra-body communication human body implantable sensor network," in *Advances in Intelligent and Soft Computing*. Springer Berlin Heidelberg, 2012, pp. 147–152.
- [10] W. J. Tomlinson *et al.*, "Galvanic coupling intra-body communication link for real-time channel assessment," in *IEEE INFOCOM Workshops*, 2016.
- [11] Y. Xu *et al.*, "Modeling and Characterization of Capacitive Coupling Intrabody Communication in an In-Vehicle Scenario," *Sensors*, vol. 19, p. 4305, oct 2019.
- [12] A. Datta *et al.*, "Advanced biophysical model to capture channel variability for eqs capacitive hbc," *bioRxiv*, 2020.
- [13] Y. K. Hernandez-Gomez *et al.*, "Magnetic human body communication based on double-inductor coupling," in *IEEE I2MTC*, vol. 9, 2017, pp. 1–6.
- [14] S. Banou *et al.*, "MAGIC: Magnetic Resonant Coupling for Intra-body Communication," in *IEEE INFOCOM*, vol. 2020-July, 2020, pp. 1549–1558.
- [15] T. G. Zimmerman, "Personal area networks: Near-field intrabody communication," *IBM Systems Journal*, vol. 35, pp. 609–617, 1996.
- [16] J. Park *et al.*, "Magnetic human body communication," in *IEEE EMBC*, 2015, pp. 1841–1844.
- [17] T. Handa *et al.*, "A very low-power consumption wireless eeg monitoring system using body as a signal transmission medium," in *Transducers*, vol. 2, 1997, pp. 1003–1006.
- [18] D. P. Lindsey *et al.*, "A new technique for transmission of signals from implantable transducers," *IEEE transactions on biomedical engineering*, vol. 45, pp. 614–619, 1998.
- [19] K. Hachisuka *et al.*, "Development and performance analysis of an intra-body communication device," in *Transducers*, vol. 2, 2003, pp. 1722–1725.
- [20] M. S. Wegmueller *et al.*, "Signal transmission by galvanic coupling through the human body," *IEEE Transactions on Instrumentation and Measurement*, vol. 59, pp. 963–969, 2010.
- [21] M. A. Callejon *et al.*, "Galvanic coupling transmission in intrabody communication: A finite element approach," *IEEE Transactions on Biomedical Engineering*, vol. 61, pp. 775–783, 2013.
- [22] F. Koshiji *et al.*, "Wireless body area network using magnetically-coupled wearable coils," in *IEEE ICSJ*, 2015, pp. 208–211.
- [23] K. Agarwal *et al.*, "Wireless power transfer strategies for implantable bioelectronics," *IEEE Reviews in Biomedical Engineering*, vol. 10, pp. 136–161, 2017.
- [24] D. Xianyi *et al.*, "Reduction in human interaction with magnetic resonant coupling wpt systems with grounded loop," *Energies*, vol. 14, p. 7253, 11 2021.
- [25] U. S. R. Peripheral, "Universal software radio peripheral," <http://www.ettus.com/>, accessed: Aug 2021.
- [26] R. University, "Warp: Wireless open-access research platform," <http://warpproject.or>, accessed: Aug 2021.
- [27] N. Semiconductors, "Nxp nfmi radio nxh2280," <http://www.nxp.com/documents/leaflet/75017645.pdf>, accessed: March 18th, 2016.
- [28] M. Bailleul, "Shielding of the electromagnetic field of a coplanar waveguide by a metal film: Implications for broadband ferromagnetic resonance measurements," *Applied Physics Letters*, vol. 103, p. 192405, Nov. 2013. [Online]. Available: <https://doi.org/10.1063/1.4829367>
- [29] S. Islam *et al.*, "Performance evaluation of magnetic resonance coupling method for intra-body network (IBNet)," *IEEE Transactions on Biomedical Engineering*, 2021.
- [30] "Guidelines for limiting exposure to time-varying electric and magnetic fields (1 Hz TO 100 kHz)," International Commission on Non-Ionizing Radiation Protection, Tech. Rep. 6, 2010.
- [31] "IEEE standard for safety levels with respect to human exposure to electric, magnetic, and electromagnetic fields, 0 hz to 300 GHz," 2019. [Online]. Available: <https://doi.org/10.1109/ieeestd.2019.8859679>
- [32] M. Jacobsson *et al.*, "Estimating packet delivery ratio for arbitrary packet sizes over wireless links," *IEEE Communications Letters*, vol. 19, pp. 609–612, 2015.